RSC Advances

PAPER

View Article Online
View Journal | View Issue

Cite this: *RSC Adv.*, 2026, **16**, 29240

Chemical epigenetic modification uncovers new isocoumarins from the endophyte *Dothideomycetes* sp. BMC-101

Yajuan Cong,†[a] Haotian Wang,†[ab] Hong Wang,[a] Jing Jiang,[a] Lanying Li,[a] Runyu Wu,[a] Yixuan Zhang,[a] Qiang Huo*[ab] and Meilin Zhu*[ab]

Received 27th March 2026
Accepted 19th May 2026

DOI: 10.1039/d6ra02544g

rsc.li/rsc-advances

Four new isocoumarin derivatives including two pair of enantiomers [(±)- dothideomarins A (**1a**/**1b**) and B (**2a**/**2b**)], as well as two related analogs, dothideomarins C and D (**3** and **4**), were isolated from the endophytic fungus *Dothideomycetes* sp. BMC-101 obtained from *Magnolia grandiflora* L. by applying the OSMAC (One Strain Many Compounds) strategy combined with MS/MS-based molecular networking. The enantiomeric pairs existed as racemic or partially racemic mixtures and were obtained by chiral HPLC separation. Their structures were elucidated by comprehensive spectroscopic data analysis, single-crystal X-ray diffraction, and comparison of the experimental and computed ECD curves. Biological screening of all the compounds found that compounds **1a** and **2a** exhibited moderate to weak cytotoxic activity against U87, A549, SW1990 and HCT-116 cells lines, with IC_{50} values ranging from 31.9 to 48.1 μM.

1 Introduction

Natural products remain a pivotal resource for the discovery of novel bioactive compounds and pharmacophores.[1,2] Endophytic fungi represent a particularly rich source, harboring a diverse array of biologically active secondary metabolites.[3,4] However, genomic analyses indicate that a substantial number of biosynthetic gene clusters (BGCs) in fungi remain transcriptionally silent under standard laboratory culture conditions.[5] To access this hidden chemical potential, various strategies have been developed, including heterologous expression and the manipulation of pathway-specific regulators.[6–8] Among these, the "One Strain Many Compounds" (OSMAC) approach, has proven highly effective in activating silent BGCs and yielding structurally unique and/or bioactive molecules.[9] To date, OSMAC has facilitated the discovery of numerous microbial natural products spanning various classes, including cyclic peptides, alkaloids, polyketides, and terpenoids.[10,11] Typically, the OSMAC strategy incorporates methods such as variation of medium composition, variation of culture condition, cocultivation, and chemical epigenetic modification. In particular, chemical epigenetic manipulation by supplementing fungal culture mediums with some small molecular epigenetic modifying agents, such as DNA methyltransferase (DNMT) inhibitors and histone deacetylase (HDAC) inhibitors, has been an effective approach to unlock cryptic metabolites and discover new or previously unexpressed secondary metabolites.[12] SAHA (suberoylanilide hydroxamic acid) is a class I/II HDAC inhibitor. In fungi, histone acetylation/deacetylation regulates chromatin structure and gene expression. Inhibition of HDAC by SAHA leads to hyperacetylation of histones, which relaxes chromatin and facilitates the transcription of otherwise silent biosynthetic gene clusters (BGCs).[13,14]

In our initial studies, an endophytic fungus, *Dothideomycetes* sp. BMC-101 was isolated from samples of *Magnolia grandiflora* L. collected from Bengbu Medical University, China.[15] A detailed chemical investigation of this strain led to the discovery of dothideomins A–D, a series of previously undescribed bisanthraquinones featuring a unique cage-like 6/6/6/5/6/6/6 heptacyclic or 6/6/6/5/6/3/6/6 octocyclic scaffold.[16,17] To further explore the metabolic potential of this strain, the OSMAC strategy, conducting a series of experiments including variation of medium composition and chemical epigenetic modification were carried out to activate the silent biosynthetic pathways of *Dothideomycetes* sp. BMC-101.

Notably, the addition of SAHA induced the most significant alteration in the metabolic profile of *Dothideomycetes* sp. BMC-101, as monitored by HPLC-UV analysis. The results showed that the known dothideomins A–D could be identified from both samples (with and without SAHA), while peaks within 17.5–19.5 min were markedly enhanced with SAHA, indicating that a silent biosynthetic gene cluster (BGC) might be activated by the addition of SAHA (Fig. S1). Consequently, a large-scale fermentation was performed using solid medium supplemented with SAHA at a final concentration of 400 nM. Guided by molecular networking, four new compounds, designated

[a]*School of Pharmacy, Bengbu Medical University, 2600 Donghai Avenue, Bengbu 233030, Anhui, China. E-mail: 620793985@qq.com; meilin0402@bbmu.edu.cn*

[b]*Anhui Engineering Technology Research Center of Biochemical Pharmaceutical, Bengbu Medical University, 2600 Donghai Avenue, Bengbu 233030, Anhui, China*

† These authors contributed equally to this work.

dothideomarins A–D (**1–4**), were isolated. These included two pairs of racemic isocoumarins: (−)-dothideomarin A (**1a**)/(+)-dothideomarin A (**1b**) and (−)-dothideomarin B (**2a**)/(+)-dothideomarin B (**2b**). The details of the isolation, structural elucidation, and activities of compounds **1–4** were described herein.

2 Materials and methods

2.1. General experimental procedures

Optical rotations were measured on a Bellingham Stanley ADP450 digital polarimeter. Spectra were recorded on a Shimadzu UV-2700 spectrophotometer. IR spectra were obtained with a Nicolet iS50 FT-IR spectrophotometer in KBr discs. The ECD spectra were measured on a JASCO J-715 spectropolarimeter. ^{1}H NMR, ^{13}C NMR and 2D NMR spectra were recorded on an Agilent DD2-500 spectrometer, and a JNM-ECZ600/S1 600 MHz spectrometer with tetramethylsilane (TMS) as an internal standard. HRESIMS spectra were obtained by using a Thermo Scientifc Q Exactive mass spectrometer in positive and negative ionization mode. Column chromatography (CC) was performed with silica gel (200–300 mesh, Qingdao Marine Chemical Inc.) and Sephadex LH-20 (Amersham Biosciences). Semipreparative HPLC was carried out using a Shimadzu LC 20 instrument (Shimadzu Corporation, Tokyo, Japan) equipped with a multiple wavelength diode array detector (DAD) and employing a C18 reversed-phase column (Welch Ultimate XB-C_{18}, 10 × 250 mm, 5 μm). Chiral high-performance liquid chromatography (HPLC) was carried out using a Shimadzu LC 16 instrument (Shimadzu Corporation, Tokyo, Japan) with Chiralpak AD-H or OD-H columns (Daicel, 4.6 × 250 mmL, 5 μm). LC-MS was performed using an Acquity UPLC H-Class coupled to an SQ Detector 2 mass spectrometer using a BEH C_{18} column (1.7 μm, 2.1 × 50 mm, 1 mL min^{-1}) (Waters Corporation). All solvents used in CC and HPLC were of analytical grade and chromatographic grade (Shanghai Tian Scientific Co., Ltd China). All cell lines were purchased from Wuhan Procell Life Sciences Co., Ltd.

2.2. Fungal material

Dothideomycetes sp. BMC-101 (GenBank entry MZ773501) was isolated from the *Magnolia grandiflora* L. leaves which were collected from Bengbu Medical University (Bengbu, Anhui Province, 32°57′3″N, 117°21′19″E) and identified based on internal transcribed spacer (ITS) DNA sequencing.[15,16] The strain was deposited at the Anhui Engineering Technology Research Center of Biochemical Pharmaceutical, Bengbu Medical University, Bengbu, Anhui, China.

2.3. OSMAC study, fermentation, and extraction

Based on the OSMAC strategy, five different media, labeled as Fungus 2$^{\#}$ solid media (maltose 2%, mannitol 2%, glucose 1%, sodium glutamate 1%, yeast extract 0.3%, corn syrup 0.1%, KH_2PO_4 0.05%, and $MgSO_4 \cdot 7H_2O$ 0.03%, agar powder 2%, deionized water), Fungus 1$^{\#}$ solid media (sorbitol 2%, maltose 2%, sodium glutamate 1%, yeast extract 0.3%, $MgSO_4 \cdot 7H_2O$ 0.03%, tryptophan 0.05%, KH_2PO_4 0.05%, agar powder 2%, deionized water), Soy flour media (starch 2%, bean powder 1.5%, peptone 0.2%, yeast extract 0.2%, deionized water), Fungus 2$^{\#}$ solid media adding SAHA (dissolved in DMSO with a final concentration of 400 nM) and Fungus 2$^{\#}$ solid media adding valproic acid (VPA) (dissolved in DMSO with a final concentration of 400 nM) were utilized to culture the strain *Dothideomycetes* sp. BMC-101 under static condition. HPLC analysis of the extracts cultured in Fungus 2$^{\#}$ solid media adding SAHA displayed new major peaks with unusual UV absorptions, suggested that SAHA could activate the silent gene clusters and induced the production of new metabolites in *Dothideomycetes* sp. BMC-101(Fig. S1).·As a classic histone deacetylase (HDAC) inhibitor, SAHA has been widely reported to effectively activate silent biosynthetic gene clusters and promote the production of polyketide metabolites in endophytic fungi.[13,14] Therefore, the Fungus 2$^{\#}$ solid media adding SAHA was selected as the optimal conditions for large-scale fermentation. The fungus was cultured in 1L Erlenmeyer flasks each containing 300 mL of Fungus 2$^{\#}$ solid media adding SAHA at room temperature for 30 days. The whole fermented cultures (150 flasks) were crushed and then extracted three times with a mixture of 80% methanol and water. The methanol solution was evaporated under reduced pressure to afford an aqueous solution, which was then extracted with EtOAc three times. All EtOAc solutions were combined and concentrated under reduced pressure to obtain an extract (35 g).

2.4. LC-MS/MS and molecular networking analysis

Four fractions obtained from crude extracts after separating by a silica gel column chromatography were performed on an UHPLC system (Ultimate 3000, Thermo Scientific) with a C18 column (ACQUITY UPLC BEH 1.7 μm, 2.1 × 100 mm, Waters) coupled to hybrid quadrupole-Orbitrap mass spectrometer (QExactive, Thermo Scientific). The mobile phase consisted of H_2O + 0.1% formic acid (A) and HPLC-grade methanol (B). The gradient elution was maintained in 10% B for 1 min; from 10% B to 100% B in 22 min; maintained in 100% B for 3 min and then returned to initial conditions in 1 min; hold at 10% B for 3 min to re-equilibrate the column, totaling 30 min, with a flow rate of 0.25 mL min^{-1}. The injection volume was 3 μL, during the acquisition of positive polarity. The positive mode SI conditions were spray voltage, + 3.5 kV; capillary temperature, 320 °C; probe heater temperature, 300 °C; sheath gas flow rate, 40 arbitrary unites; auxiliary gas flow rate, 8 arbitrary unites; an S-Lens RF level, 50 eV. Scan range, *m*/*z* 70–1000; scan mode, full MS (resolution 70 000) and MS/MS (resolution 17 500).

The MS/MS raw data were converted to .mzML format files by using MS Convert software.[18] The molecular network was performed using the GNPS (https://gnps.ucsd.edu) data analysis workflow and the spectral clustering algorithm.[19,20] The data were filtered by removing all MS/MS fragment ions within ± 17 Da of the precursor *m*/*z*. A mass tolerance for both the precursor ion and the MS/MS fragment ion was set to 0.02 Da. The minimum pairs' cosine score were set to 0.65. MS/MS spectra were window filtered by choosing only the top 6

Table 1 ^{1}H and ^{13}C NMR data of **1–4** (δ in ppm, J in Hz)

	1a and **1b**[a]		**2a** and **2b**[b]		**3**[c]		**4**[a]	
No.	δ_C, type	δ_H (J in Hz)	δ_C, type	δ_H (J in Hz)	δ_C, type	δ_H (J in Hz)	δ_C, type	δ_H (J in Hz)
1	170.2, C		170.1, C		166.7, C		170.5, C	
3	76.6, CH	4.75, m	74.7, CH	4.99, m	75.8, CH	4.69, m	76.3, CH	4.68, m
4	29.7, CH_2	*a*: 2.99, dd (16.6, 3.4) *b*: 2.72, dd (16.5, 11.4)	30.8, CH_2	*a*: 3.11, dd (17.3, 5.6) *b*: 2.83, dd (17.3, 6.5)	31.2, CH_2	*a*: 3.04, dd (17.0, 3.0) *b*: 2.79, dd (17.0, 11.5)	29.9, CH_2	*a*: 2.99, dd (16.8, 3.4) *b*: 2.74, dd (16.7, 11.6)
4a	135.2, C		133.5, C		145.6, C		135.5, C	
5	124.4, C		124.9, C		125.4, C		125.0, C	
6	138.6, CH	7.27, s	139.1, CH	7.17, s	138.0, CH	7.84, s	139.2, CH	7.28, s
7	123.1, C		124.3, C		115.7, C		123.8, C	
8	157.6, C		158.9, C		160.4, C		158.1, C	
8a	107.3, C		107.3, C		111.2, C		107.9, C	
10	43.9, CH_2	*a*: 1.83, m *b*: 1.67, m	48.01, CH_2	*a*: 3.04, dd (16.2, 3.4) *b*: 2.70,dd (16.4, 11.6)	44.2, CH_2	*a*: 1.81, m *b*: 1.66, m	40.9, CH_2	2.01, m
2′	61.8, CH	3.90, m	204.4, C		62.2, CH	3.89, m	67.0, CH	5.04, m
3′	24.2, CH_3	1.12, d (6.2)	29.8, CH_3	2.25, s	24.7, CH_3	1.11, d (6.1)	20.8, CH_3	1.24, d (6.3)
5-CH_3	14.8, CH_3	2.13, s	15.2, CH_3	2.21, s	18.1, CH_3	2.20, s	18.0, CH_3	2.14, s
7-COOH/CH_3	17.4, CH_3	2.13, s	17.9, CH_3	2.15, s	168.9, C		15.5, CH_3	2.13, s
8-OH		11.19, s		11.07, s				11.12, s
2′-OCO$\underline{C}H_3$							170.6, C	
2′-OCO$\underline{CH}_3$							21.5, CH_3	1.98, s

[a] Data were measured at 600 MHz for ^{1}H NMR and 150 MHz for ^{13}C NMR in DMSO-d_6. [b] Data were measured at 500 MHz for ^{1}H NMR and 125 MHz for ^{13}C NMR in $CDCl_3$. [c] Data were measured at 500 MHz for ^{1}H NMR and 125 MHz for ^{13}C NMR in DMSO-d_6.

fragment ions in the ± 50 Da window throughout the spectrum. The minimum cluster size was set to 1. The network TopK was set to 10. MS/MS nodes with precursor ion abundance > 1×10^4 and minimum MS/MS intensity of 500 were included. The spectra network was visualized using Cytoscape 3.9.1 software.[21] The molecular networking job can be found at the following link: https://gnps.ucsd.edu/ProteoSAFe/status.jsp?task=4e432a078a2e471087b891b94cc1a107.

2.5. Isolation and purifcation

The extract was fractionated on a Rp-C18 column using gradient elution with MeOH–H_2O (10 : 90, 30 : 70, 50 : 50, 70 : 30, v/v), led to the separation of four fractions (Frs. A–D). Fr. D was separated by Si gel vacuum liquid chromatography (VLC) using a stepped gradient elution of petroleum ether (PE)- ethyl acetate (EA) (from 100 : 1 to 10 : 1) to yield five subfractions (Frs. D1–D5). Fr. D3 was set to VLC with a PE–EA gradient (from 100 : 1 to 1 : 20) to yield four subfractions (Frs. D3.1–D3.5). Fr. D3.2 was purified by semipreparative HPLC (32% CH_3CN–H_2O, 3 mL min^{-1}) to give **3** (30 mg, t_R 18.4 min). Fr. D4 was purified by Sephadex LH-20 (MeOH) to afford three subfractions (Frs. D4.1–D4.3). Fr.D4.2 was further purified by semipreparative HPLC (50% CH_3CN–H_2O, 3 mL min^{-1}), affording a racemic mixture of compounds **1** (9 mg, t_R 26.5 min). A part of the mixture was further purified by chiral HPLC over a Daicel Chiralpak OD-H column eluted with *n*-hexane and 2-propanol (90 : 10) to yield enantiomeric pure isomers **1a** (2.1 mg, t_R 8.7 min) and **1b** (2.2 mg, t_R 10.5 min). Fr.D4.1 was also subjected to semi-preparative HPLC (50% CH_3CN–H_2O, 3 mL min^{-1}) to give a racemic mixture of **2** (20 mg, t_R 25 min). A part of the mixture was further purified by chiral HPLC over a Daicel Chiralpak AD-H column eluted with *n*-hexane and 2-propanol (96 : 4) to yield enantiomeric pure isomers **2a** (2.1 mg, t_R 16.7 min) and **2b** (2.2 mg, t_R 18.3 min). Subsequently, Fr. D5 was separated using an VLC with a PE–EA gradient (from 50 : 1 to 1 : 1), followed by semipreparative HPLC (78% CH_3CN–H_2O, 3 mL min^{-1}) to yield **4** (8.8 mg, t_R 29.2 min).

2.5.1 (±)-Dothideomarin A (1). Colorless crystals (CH_2Cl_2–MeOH = 1 : 1); UV (MeOH) λ_{max} (log ε): 211 (4.10), 253 (3.60), 330 (3.40), nm; IR (KBr) ν_{max}: 3201, 1701, 1600, 1450, 1432, 1200, 1153, 1077, 800, 701 cm^{-1}; ^1H and ^{13}C NMR data (DMSO-d_6) see Table 1; HRESIMS *m*/*z* 251.1283 $[M + H]^+$ (calcd for $C_{14}H_{19}O_4$, 251.1278).

2.5.2 (−)-Dothideomarin A (1a). $[\alpha]_D^{25}$ = −30.9 (*c* 0.1, MeOH), ECD (MeOH) λ_{max} ($\Delta\varepsilon$): 207 (+9.89), 234 (−2.88), 261 (+7.89), 290 (+0.06), 320 (+1.18) nm.

2.5.3 (+)-Dothideomarin A (1b). $[\alpha]_D^{25}$ = +29.3 (*c* 0.1, MeOH), ECD (MeOH) λ_{max} ($\Delta\varepsilon$): 214 (−5.23), 233 (+1.91), 260 (−4.97), 287 (−0.34), 328 (−0.87) nm.

2.5.4 (±)-Dothideomarin B (2). Pale-yellow powder; UV (MeOH) λ_{max} (log ε): 211 (4.34), 253 (3.90), 330 (3.70) nm; IR (KBr) ν_{max}: 3228, 2892, 1710, 1600, 1500,1450, 1210, 843, 803 cm^{-1}; ^1H and ^{13}C NMR data (DMSO-d_6) see Table 1; HRESIMS *m*/*z* 249.1126 $[M + H]^+$ (cald for $C_{14}H_{17}O_4$ 249.1121).

2.5.5 (−)-Dothideomarin B (2a). $[\alpha]_D^{25}$ = −134.0 (*c* 0.1, MeOH); ECD (MeOH) λ_{max} ($\Delta\varepsilon$): 230 (−0.84), 261 (+3.02), 293 (+0.08), 320 (+0.37) nm.

2.5.6 (+)-Dothideomarin B (2b). $[\alpha]_D^{25}$ = +123.8 (*c* 0.1, MeOH); ECD (MeOH) λ_{max} ($\Delta\varepsilon$): 224 (+0.59), 235 (+0.94), 261 (−2.24), 295 (−0.33), 320 (−0.56) nm.

2.5.7 Dothideomarin C (3). Pale-yellow powder; $[\alpha]_D^{25}$ = +48.0 (*c* 0.1, MeOH); UV (MeOH) λ_{max} (log ε): 220 (4.11), 330 (3.48), nm; ECD (MeOH) λ_{max} ($\Delta\varepsilon$): 223 (+1.87), 248 (−16.10), 293 (−0.90), 329 (−2.99) nm; IR (KBr) ν_{max}: 3392, 2989, 1700, 1600, 1450, 1432, 1201, 1151, 1078, 798, 700 cm^{-1}; ^1H and ^{13}C NMR data (DMSO-d_6) see Table 1; HRESIMS *m*/*z* 279.0872 $[M–H]^+$ (calcd for $C_{14}H_{15}O_6$, 279.0874).

2.5.8 Dothideomarin D (4). Pale-yellow powder; $[\alpha]_D^{25}$ = +50.0 (*c* 0.1, MeOH); UV (MeOH) λ_{max} (log ε): 211 (4.54), 253 (4.11), 330 (3.90) nm; ECD (MeOH) λ_{max} ($\Delta\varepsilon$): 237 (+1.35), 260 (−8.93), 292 (−0.35), 328 (−0.62) nm; IR (KBr) ν_{max}: 3408, 2902, 1730, 1600, 1450, 1207, 767, 701 cm^{-1}; ^1H and ^{13}C NMR data (DMSO-d_6) see Table 1; HRESIMS *m*/*z* 293.1383 $[M + H]^+$ (calcd for $C_{16}H_{21}O_5$, 293.1384).

2.6. X-ray crystallographic analysis of (±)dothideomarin A (1)

Single crystals of $C_{14}H_{18}O_4$ were obtained in a mixed solution of CH_2Cl_2–MeOH (1 : 1). A suitable crystal was selected and analyzed on a Bruker APEX-II CCD diffractometer with Cu Kα radiation (λ = 1.54178 Å). The crystal was kept at 303.00 K during data collection. Using Olex2,[22] the structure was solved with the SHELXT structure solution program using Intrinsic Phasing and refined with the SHELXL refinement package using Least Squares minimization.[23] Crystallographic data have been deposited in the Cambridge Crystallographic Data Center with the number CCDC 2443606.

Crystal data of (±)-dothideomarin A (**1**): monoclinic, space group $P2_1/c$ (no. 14), a = 8.5056(3) Å, b = 39.6740(13) Å, c = 7.9424(3) Å, β = 94.882(2)°, V = 2670.45(16) $Å^3$, Z = 8, T = 303.00 K, μ(CuKα) = 0.745 mm^{-1}, D_{calc} = 1.245 g cm^{-3}, 19 445 reflections measured (4.454° ≤ 2Θ ≤ 136.784°), 4745 unique (R_{int} = 0.0389, R_{sigma} = 0.0381) which were used in all calculations. The final R_1 was 0.0674 ($I > 2\sigma(I)$) and wR_2 was 0.2007 (all data).

2.7. Computation section

Conformational searches were performed *via* molecular mechanics using the MMFF (Merck Molecular Force Field) method in Spartan'14 software.[24] To obtain the energy minimized conformers, the resultant corresponding stable conformers (rel. E < 5 kcal mol^{-1}) were collected and the geometries were reoptimized at the B3LYP/6-31+G(d) PCM/MeOH level by using the Gaussian 09 software.[25] Then, the optimized conformers of **1a** (>5% population) were subjected to the calculations of the ECD spectra using time-dependent DFT (TD-DFT) at B3LYP/6-31G(d) PCM/MeOH. The ECD spectra were generated using the program SpecDis[26] by applying a Gaussian band shape with a 0.25 eV width for **1a** from dipole-length rotational strengths.

2.8. Cytotoxicity assay

The human glioblastoma cell line U87, mouse breast cancer cell line 4T1, human lung adenocarcinoma epithelial cell line A549, human pancreatic adenocarcinoma cell line SW1990 and human colon carcinoma cell line HCT-116 were cultured in Dulbecco's modified Eagle's medium (DMEM) containing 10% fetal bovine serum (FBS) at 37 °C for 24 h in a 5% CO_2 incubator at a density of 1×10^4 cells per well. Compounds were dissolved in DMSO to prepare 10 mM solutions, then diluted with the culture medium in the 96-well plates to achieve final concentrations of 100, 50, 20, 10, 5, 1, and 0.1 μM. After 24 h of incubation, the Cell Counting Kit-8 (biosharp) reagent was added to the medium and incubated for 2 h. Cell viability was measured by absorbance at 450 nm using the Agilent Biotek epoch 2 microplate reader. The inhibitory rate of cell proliferation was expressed as IC_{50} values. Cisplatin was used as a positive control and cell solutions containing 0.5% DMSO served d as a negative control.

2.9. Antibacterial activity

Antibacterial activities of compounds were evaluated against Methicillin-resistant *Staphylococcus aureus* ATCC 43300 (MRSA), *Staphylococcus aureus* ATCC 29213, *Bacillus subtilis* ATCC 6051, and *Acinetobacter baumannii* AB34. Tetracycline was used as a positive control. The detailed methodologies for biological testing have been described in a previous report.[16,27]

3 Results and disscussion

The fermentation broth and mycelia of *Dothideomycetes* sp. BMC-101, cultured on Fungus 2# solid medium supplemented with SAHA, were exhaustively extracted with EtOAc. The resulting organic extract was fractionated by column chromatography to yield four subfractions (Frs. A–D). To avoid the repeated isolation of known constituents, these sub-fractions were analyzed by LC-MS/MS, and the data were used to construct an MS/MS-based molecular network (MN) on the Global Natural Products Social Molecular Networking (GNPS) platform (https://gnps.ucsd.edu; Fig. 1). Interestingly, the GNPS analysis revealed an uncharacterized cluster of 9 nodes (with *m*/*z* values between 229 and 325) in Fraction D displayed distinct UV profiles ($\lambda_{max} \sim 220$, 330 nm or 211, 253, 330 nm), which differed clearly from those of the previously reported dothideomins ($\lambda_{max} \sim 207$, 248, 311, 380 nm) isolated from the same strain.[16] Moreover, there were no references in the GNPS spectral libraries that matched with this molecular family, suggesting that these compounds may be new compounds.

Compound **1** was obtained as colorless crystals. Its molecular formula was established as $C_{14}H_{18}O_4$ on the basis of the HRESIMS data at *m*/*z* 251.1283 $[M + H]^+$ (calcd for $C_{14}H_{19}O_4$, 251.1278), indicating 6 degrees of unsaturation. The ^1H NMR spectroscopic data of **1** revealed the presence of a chelated hydroxyl group (δ_H 11.15, 8-OH), an aromatic proton (δ_H 7.24, H-6), two oxygenated methine protons (δ_H 4.72 and 3.87, H-3 and H-2′), two methylene protons (δ_H 2.95 and 2.69, H_2-4; δ_H 1.80 and 1.62, H_2-1′), and three methyl groups (δ_H 2.11, 5-CH_3; δ_H 2.11,7-CH_3; δ_H 1.10, H_3-3′). Inspection of the ^{13}C NMR spectrum exhibited 14 carbon signals for three methyls, two methylenes, two sp^3 and one sp^2 methines, and six quaternary carbons. Detailed analysis of the ^1H and ^{13}C NMR data (Table 1) suggested that **1** belongs to the isocoumarin family. The HMBC correlations from aromatic proton H-6 to C-4a, C-8, and 5-CH_3, from the chelated hydroxyl group 8-OH to C-7 and C-8a, from 7-CH_3 to C-6 and C-7, from the oxygenated methine proton H-3 to C-1 and C-4a, and from the methylene protons H_2-4 to C-5 and C-8a further established the isocoumarin core as identical to that of the known compound 3*R*-(2*R*-hydroxypropyl)-8-hydroxyl-7-methyl-3,4-dihydroisocoumarine[28](Fig. 2). A notable structural difference was the replacement of the aromatic proton H-5 in the known compound with a methyl group in **1** which was supported by the HMBC correlations from 5-CH_3 to C-5 and C-4a. Furthermore, the COSY correlations of H_2-4/H-3/H_2-1′/H-2′/H_3-3′ indicated the presence of a 2-hydroxypropyl side chain at C-3, consistent with the HMBC correlation from H_2-1′ to C-4 (Fig. 3). Thus, the planar structure of compound **1** was determined as shown.

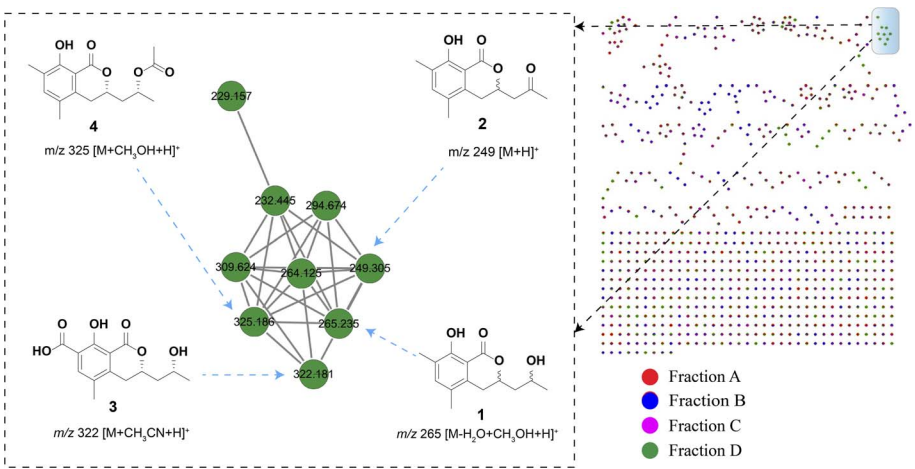

Fig. 1 Partial molecular network of metabolites from extracts of *Dothideomycetes* sp. BMC-101 and visualized with cytoscape 3.9.1 software.

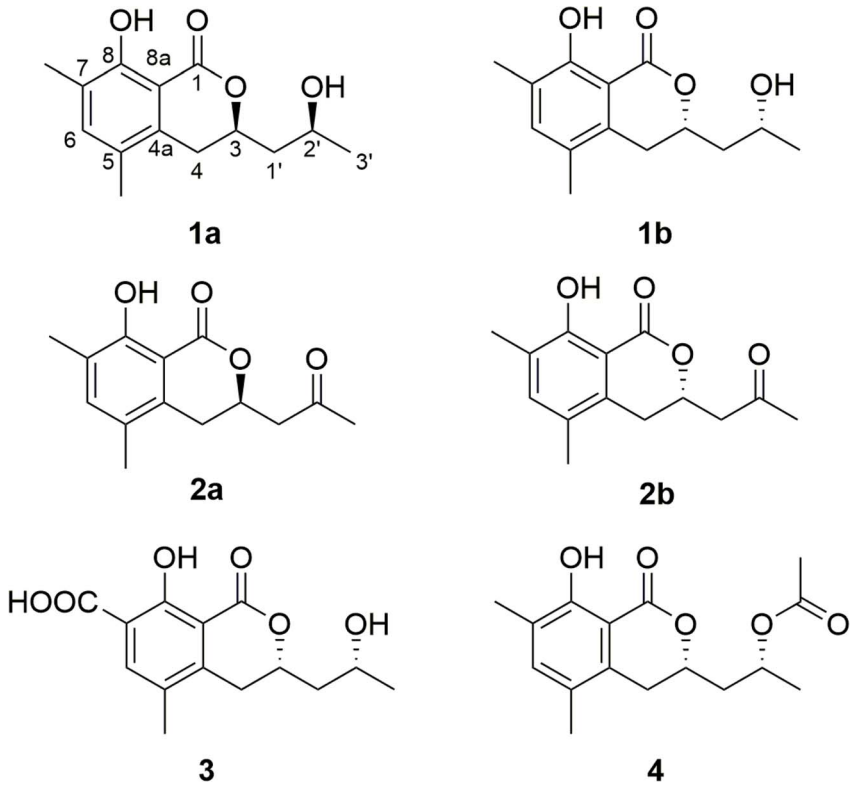

Fig. 2 Structures of compounds 1–4.

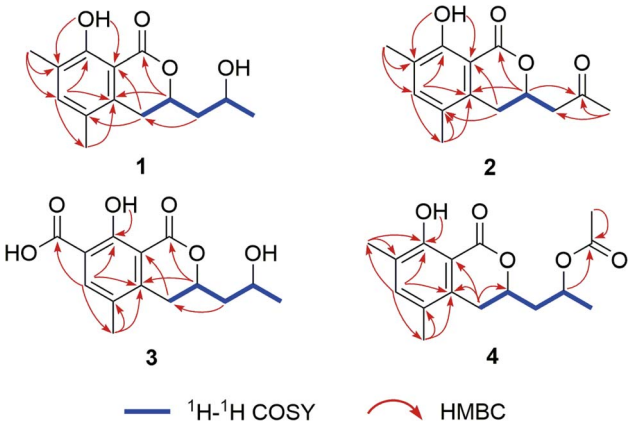

Fig. 3 Key HMBC, COSY, correlations of compounds 1–4.

The NOESY spectrum of **1** showed cross-peaks between H-3 and H-2′, indicating their spatial proximity on the same face of the molecule (Fig. 4). Fortunately, suitable crystals for X-ray diffraction were obtained, and a single-crystal X-ray crystallography (Cu Kα radiation) confirmed the planar structure and relative configuration of **1** (Fig. 5). Based on the crystal structure (CCDC: 2443606, Cu Kα), **1** was proposed to be a racemic mixture. Subsequent chiral HPLC separation using a Daicel Chiralpak OD-H column yielded a pair of enantiomers, **1a** and **1b**, in an approximate ratio of 1 : 2 (Fig. S2). The absolute configurations of **1a** and **1b** were determined by time-dependent density functional theory (TDDFT) ECD calculations. The MMFF-generated conformers of the proposed 3R, 2′S-configuration (**1a**) were reoptimized at the B3LYP/6-31G(d) level with the PCM/MeOH solvent model. Four conformers accounting for >5% Boltzmann population were obtained (Fig. S3). The calculated ECD spectrum for 3*R*, 2′*S*-**1** (**1a**) matched well with the experimental ECD spectrum of **1a**, while the calculated spectrum for the enantiomer 3*S*, 2′*R*-**1** corresponded closely to that of **1b** (Fig. 6). Combining the single-crystal X-ray diffraction result with the agreement between calculated and experimental ECD spectra, the absolute

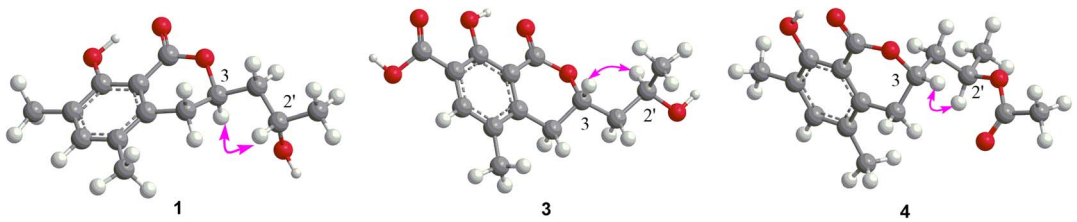

Fig. 4 Key NOESY correlations of compounds 1, 3 and 4.

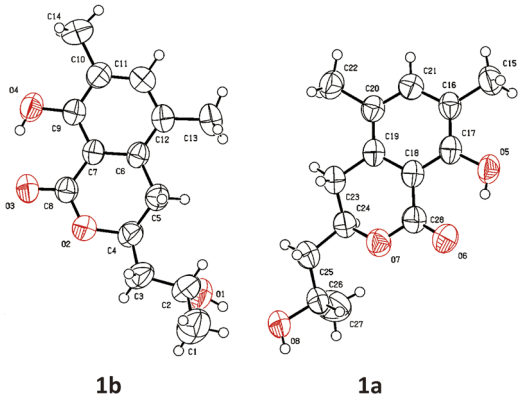

Fig. 5 Single-crystal X-ray structure of **1** (CDCC: 2443606).

configurations were assigned as 3*R*, 2′*S* for **1a** and 3*S*, 2′*R* for **1b**. Accordingly, compound **1** was identified as (±)-dothideomarin A.

Compound **2** was obtained as a white powder, having the molecular formula $C_{14}H_{16}O_4$ based on the HRESIMS at *m*/*z* 249.1126 $[M + H]^+$ (cald for $C_{14}H_{17}O_4$ 249.1121). The ^{1}H NMR data revealed the presence of protons for one chelated phenolic hydroxyl, one aromatic, one oxygenated methine, two methylenes and three methyls. Comparison of the ^{13}C NMR data of **2** with those of **1** indicated that both compounds share the same core scaffold, with the key difference being the oxidation of the 2′-OH group in **1** to a carbonyl in **2** (δ_C 204.4 *vs.* δ_C 62.3 in **1**). This structural assignment was further supported by the HMBC correlations from H_3-3′ to C-1′ and C-2′ and from H-3 to C-2′ (Table 1 and Fig. 3). Despite the existence of a stereocenter at C-3 in the molecule, compound **2** was obtained as an optically inactive substance, suggesting it was also a racemic mixture. Subsequently, Chiral HPLC separation using a Daicel Chiralpak AD-H column afforded a pair of enantiomers, **2a** and **2b**, in an approximate 1 : 1 ratio (Fig. S2). Their enantiomeric relationship was confirmed by their opposite specific rotations ($[\alpha]_D^{25}$ −134.0 for **2a** and +123.8 for **2b**) and mirror-image ECD spectrum. Finally, the absolute configurations of each enantiomer were determined as 3*R* for (−)-**2a** and 3*S* for (+)-**2b**, by comparing their experimental ECD spectra with those of (−)-**1a** and (+)-**1b**, respectively (Fig. 6).

Compound **3** was isolated as a white powder. The molecular formula was determined to be $C_{14}H_{16}O_6$ by the negative HRESIMS ion at *m*/*z* 279.0872 $[M–H]^+$ (calcd for $C_{14}H_{15}O_6$, 279.0874), indicated seven degrees of unsaturation. Comparison of the ^{1}H and ^{13}C NMR data (Table 1) with those of **1** showed the presence of the same isocoumarin framework, except for one of the methyl group (7-CH_3) in **1** being replaced by a carboxyl group in **3**. This modification was supported by the HMBC correlation from H-6 to 7-COOH, as well as the characteristic chemical shift of 7-COOH (δ_C 168.9) (Table 1 and Fig. 3). Accordingly, the planar structure of **3** was elucidated as depicted. Inspired by the specific rotation value of $[\alpha]_D^{25}$ +48.0 (*c* 0.1, MeOH) together with chiral HPLC analysis, **3** was considered to be a single enantiomer, distinct from the racemic mixtures **1** and **2**. The NOESY correlation between H-3 and H-2′ and the similarity of its ECD spectrum to that of **1b** allowed the absolute configuration of **3** to be assigned as 3*S*, 2′*R* (Fig. 4 and 6).

Compound **4** was obtained as a white powder and exhibited optical activity with a specific rotation of $[\alpha]_D^{25}$ +50.0 (*c* 0.1, MeOH). The molecular formula of **4** was deduced as $C_{16}H_{20}O_5$ by the HRESIMS ion at *m*/*z* 293.1383 $[M + H]^+$ (calcd for $C_{16}H_{21}O_5$, 293.1384). Analysis of the ^{1}H and ^{13}C NMR data of **4** indicated a structure highly similar to that of **1**, with the key difference being the replacement of the hydroxyl group at C-2′ in **1** by an acetoxyl moiety in **4** (δ_C 170.6, 2′-OCOCH$_3$; δ_H 1.98, 2′-OCOCH$_3$; δ_C 21.5, 2′-OCOCH$_3$). The above assignment was corroborated by the HMBC correlations (Table 1 and Fig. 3). Therefore, the planar structure of **4** was established. The NOESY correlation between H-3 and H-2′ suggested their spatial proximity, consistent with the relative configuration observed in **3**. Based on biosynthetic considerations and a comparison of its experimental ECD spectrum with those of **1a** and **1b**, the absolute configuration of **4** was assigned as 3*S*, 2′*R* (Fig. 6).

The new compounds (**1–4**) were evaluated for cytotoxic activities against five human cancer cell lines (U87: human astrocytic glioblastoma cells; 4T1: Mouse Breast Cancer Cells; A549: human lung adenocarcinoma cells; SW1990: human pancreatic cancer cells; HCT-116: Human colon cancer cells)

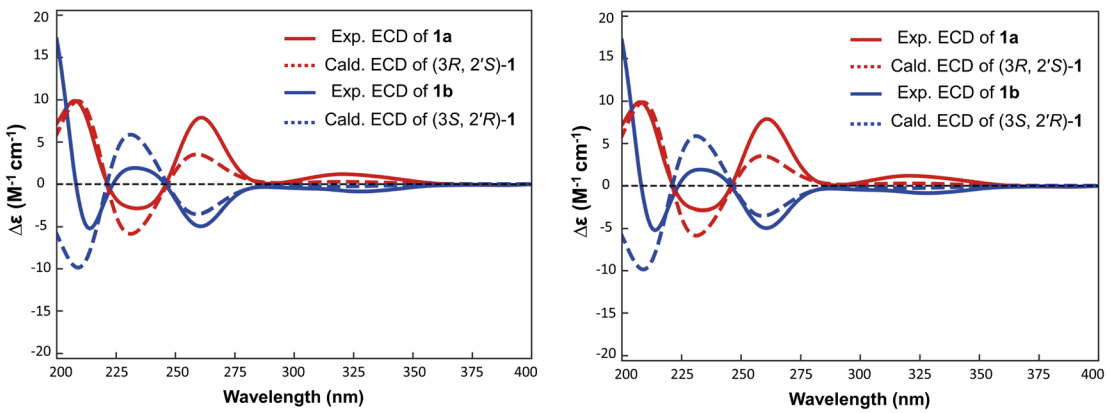

Fig. 6 ECD spectra of **1–4**. (left) Experimental and calculated ECD spectra of **1a** and **1b**. (right) experimental ECD spectra of **1a**, **1b**, **2a**, **2b**, **3** and **4**.

Table 2 Cytotoxic effects of compounds **1–4** against five cancer cell lines

	IC_{50} (μM)				
Compound	U87	4T1	A549	SW1990	HCT-116
1a	34.1	>50.0	48.1	47.4	31.9
1b	>50.0	>50.0	>50.0	>50.0	>50.0
2a	>50.0	>50.0	>50.0	35.1	>50.0
2b	>50.0	>50.0	>50.0	>50.0	>50.0
3	>50.0	>50.0	>50.0	>50.0	>50.0
4	>50.0	>50.0	>50.0	>50.0	>50.0
Cisplatin	7.5	>50.0	24.5	15.9	40.4

using CCK8 methods with cisplatin as a positive control. Only compounds **1a** and **2a** showed moderate cytotoxic activity against at least one of the above cells with IC_{50} values ranging from 31.9 to 48.1 μM (Table 2), suggesting that the 3*R* configuration was advantageous to 3*S* for cytotoxicity. In addition, acetylation of the 2′-OH (**4**) resulted in inactivity, indicating that a free 2′-OH may be essential for the activity.

Compounds **1–4** were also tested for antibacterial activities toward seven indicated strains, including Methicillin-resistant *Staphylococcus aureus* ATCC 43300 (MRSA), *Staphylococcus aureus* ATCC 29213, *Bacillus subtilis* ATCC 6051 and *Acinetobacter baumannii* AB34. However, none of the tested isocoumarins showed detectable antibacterial activity against these strains, indicating that compounds discovered in this study may lack the key pharmacophore features necessary for antibacterial activity. For example, exserolides F,[29] which possesses a hydroxyl substitution at C-5, exhibits inhibitory effects against *Staphylococcus aureus* and *Escherichia coli*, with the minimum MIC value as low as 0.16 μg mL^{-1}. In contrast, the compounds in this study bear a methyl substitution at C-5 instead of a hydroxyl group, and this structural difference may be an important reason for their loss of antibacterial activity.

4 Conclusions

In conclusion, isocoumarins are a class of natural lactones widely distributed in microorganisms and plants.[30,31] Their characteristic benzopyrone skeleton, often substituted with hydroxy and methoxy groups, confers a broad spectrum of biological activities—including antibacterial, anti-inflammatory, antioxidant, and cytotoxic properties—making them promising scaffolds for pharmaceutical development.[32,33] In this study, four new isocoumarins were isolated and identified from the endophytic fungus *Dothideomycetes* sp. BMC-101 by integrating the OSMAC strategy with GNPS-guided molecular networking. The results demonstrated that the addition of the histone deacetylase inhibitor SAHA to Fungus $2^{\#}$ solid medium significantly altered the secondary metabolic profile of the fungus. Epigenetic regulation triggered by SAHA effectively activated its latent metabolic potential, significantly enriching the chemical diversity of metabolites and promoting the production of new compounds derived from distinct metabolic routes. Notably, the activation was specific to SAHA, as another HDAC inhibitor (VPA) with lower potency did not induce similar changes, suggesting that a threshold level of HDAC inhibition is required to unlock cryptic biosynthetic gene clusters (BGCs). The newly identified isocoumarins (**1–4**) are therefore likely products of a silent BGC derepressed by SAHA-mediated epigenetic modulation. Future studies including RT-qPCR analysis of key BGC genes would be employed to confirm their transcriptional upregulation upon SAHA treatment. In bioactivity evaluations, compounds **1a** and **2a** exhibited moderate cytotoxic activities with IC_{50} values ranging from 31.9 to 48.1 μM while their enantiomers (**1b** and **2b**) were inactive. This study not only enriches the structural diversity of natural isocoumarins, but also validates the high efficiency of combining epigenetic induction with molecular networking in exploring cryptic metabolites from fungi. In addition, this finding underscores the importance of absolute configuration for biological activity and suggests that the 3*R* configuration may be a critical pharmacophore for further optimization. Such enantioselective activity is rarely documented for isocoumarins and provides a valuable lead for structure–activity relationship studies.

Author contributions

Y. C.: data curation, formal analysis, investigation, writing—original draft. H. W.: methodology, software, data curation, investigation. H. W.: data curation, investigation. J. J. and L. L.: methodology, validation, formal analysis. R. W. and Y. Z.: methodology, software, data curation, formal analysis. Q. H.: resources, supervision, writing—review and editing. M. Z.: funding acquisition, methodology, project administration, resources, supervision, writing—review and editing. All authors have read and agreed to the published version of the manuscript.

Conflicts of interest

There are no conflicts to declare.

Data availability

The data supporting this article have been included as part of the supplementary information (SI). Supplementary information: Table S1: crystal data and structure refinement for (±)-(**1**). Table S2: Cartesian coordinates of the low-energy reoptimized conformer of (3*R*, 2′*S*)-**1**; Fig. S1: HPLC analysis of the crude extracts of the fungus *Dothideomycetes* sp. BMC-101 using the OSMAC strategy; Fig. S2: chiral separations of (±)-(**1**) and (±)-(**2**); Fig. S3: conformations of lowest-energy conformers of (3*R*, 2′*S*)-**1**. Fig. S4–S11: the HR-ESI-MS and NMR spectra of (±)-(**2**); Fig. S12–S18: the HR-ESI-MS and NMR spectra of **2**; Fig. S19–S6: the HR-ESI-MS and NMR spectra of **3**; Fig. S24–S30: the HR-ESI-MS and NMR spectra of **4**. See DOI: https://doi.org/10.1039/d6ra02544g.

CCDC 2443606 contains the supplementary crystallographic data for this paper.[34]

Acknowledgements

This work was funded by the Natural Science Research Project of Anhui Provincial Department of Education (2025AHGXZK30205), the Open Research Fund of Anhui Engineering Technology Research Center of Biochemical Pharmaceutical (2025SYKFD12), and the Anhui Provincial College Student Innovation and Entrepreneurship Training Program (S202510367168).

Notes and references

1 A. G. Atanasov, S. B. Zotchev, V. M. Dirsch and C. T. Supuran, *Nat. Rev. Drug Discovery*, 2021, **20**, 200–216.
2 B. Chopra and A. K. Dhingra, *Phytother. Res.*, 2021, **35**, 4660–4702.
3 Z. Wang, L. Wang, Y. Pan, X. Zheng, X. Liang, L. Sheng, D. Zhang, Q. Sun and Q. Wang, *Bioprocess Biosyst. Eng.*, 2023, **46**, 165–170.
4 A. H. Hashem, M. S. Attia, E. K. Kandil, M. M. Fawzi, A. S. Abdelrahman, M. S. Khader, M. A. Khodaira, A. E. Emam, M. A. Goma and A. M. Abdelaziz, *Microb. Cell Fact.*, 2023, **22**, 107.
5 N. Ziemert, M. Alanjary and T. Weber, *Nat. Prod. Rep.*, 2016, **33**, 988–1005.
6 P. J. Rutledge and G. L. Challis, *Nat. Rev. Microbiol.*, 2015, **13**, 509–523.
7 A. A. Brakhage, J. Schuemann, S. Bergmann, K. Scherlach, V. Schroeckh and C. Hertweck, *Prog. Drug Res.*, 2008, **66**, 1–12.
8 L. C. Pillay, L. Nekati, P. J. Makhwitine and S. I. Ndlovu, *Front. Microbiol.*, 2022, **13**, 815008.
9 Y. Zhang, L. Feng, X. Hemu, N. H. Tan and Z. Wang, *Eur. J. Med. Chem.*, 2024, **268**, 116175.
10 H. B. Bode, B. Bethe, R. Höfs and A. Zeeck, *Chembiochem*, 2002, **3**, 619–627.
11 C. Pinedo-Rivilla, J. Aleu and R. Durán-Patrón, *Mar. Drugs*, 2022, **20**, 84.
12 Y. Lai, L. Wang, W. Zheng and S. Wang, *J. Fungi*, 2022, **8**, 565.
13 K. P. Ramesha, N. Chandra Mohana, S. Chandra Nayaka and S. Satish, *Front. Microbiol.*, 2021, **12**, 730355.
14 S. Bind, S. Bind, A. K. Sharma and P. Chaturvedi, *Front. Microbiol.*, 2022, **13**, 784109.
15 L. S. Wang, S. K. Zong, P. P. Wu, X. L. Sun, C. Z. Wu, H. T. Wang and M. L. Zhu, *J. Asian Nat. Prod. Res.*, 2023, **25**, 731–740.
16 L. Wang, S. Zong, H. Wang, C. Wu, G. Wu, F. Li, G. Yu, D. Li and M. Zhu, *J. Nat. Prod.*, 2022, **85**, 2789–2795.
17 F. Zhang, C. Ma, M. Zhu, Y. Chen, W. Wang, G. Zhang, T. Zhu, Q. Che and D. Li, *J. Am. Chem. Soc.*, 2025, **147**, 7094–7102.
18 F. Olivot, G. Grelier, F. Roussi, M. Litaudon and D. Touboul, *Anal. Chem.*, 2017, **89**, 7836–7840.
19 A. T. Aron, E. C. Gentry, K. L. McPhail, L. F. Nothias, M. Nothias-Esposito, A. Bouslimani, D. Petras, J. M. Gauglitz, N. Sikora, F. Vargas, J. J. J. van der Hooft, M. Ernst, K. B. Kang, C. M. Aceves, A. M. Caraballo-Rodríguez, I. Koester, K. C. Weldon, S. Bertrand, C. Roullier, K. Sun, R. M. Tehan, P. C. A. Boya, M. H. Christian, M. Gutiérrez, A. M. Ulloa, J. A. Tejeda Mora, R. Mojica-Flores, J. Lakey-Beitia, V. Vásquez-Chaves, Y. Zhang, A. I. Calderón, N. Tayler, R. A. Keyzers, F. Tugizimana, N. Ndlovu, A. A. Aksenov, A. K. Jarmusch, R. Schmid, A. W. Truman, N. Bandeira, M. Wang and P. C. Dorrestein, *Nat. Protoc.*, 2020, **15**, 1954–1991.
20 L. F. Nothias, D. Petras, R. Schmid, K. Dührkop, J. Rainer, A. Sarvepalli, I. Protsyuk, M. Ernst, H. Tsugawa, M. Fleischauer, F. Aicheler, A. A. Aksenov, O. Alka, P. M. Allard, A. Barsch, X. Cachet, A. M. Caraballo-Rodriguez, R. R. Da Silva, T. Dang, N. Garg, J. M. Gauglitz, A. Gurevich, G. Isaac, A. K. Jarmusch, Z. Kameník, K. B. Kang, N. Kessler, I. Koester, A. Korf, A. Le Gouellec, M. Ludwig, H. C. Martin, L. I. McCall, J. McSayles, S. W. Meyer, H. Mohimani, M. Morsy, O. Moyne, S. Neumann, H. Neuweger, N. H. Nguyen, M. Nothias-Esposito, J. Paolini, V. V. Phelan, T. Pluskal, R. A. Quinn, S. Rogers, B. Shrestha, A. Tripathi, J. J. J. van der Hooft, F. Vargas, K. C. Weldon, M. Witting, H. Yang, Z. Zhang, F. Zubeil, O. Kohlbacher, S. Böcker, T. Alexandrov, N. Bandeira, M. Wang and P. C. Dorrestein, *Nat. Methods*, 2020, **17**, 905–908.
21 M. E. Smoot, K. Ono, J. Ruscheinski, P. L. Wang and T. Ideker, *Bioinformatics*, 2011, **27**, 431–432.
22 O. V. Dolomanov, L. J. Bourhis, R. J. Gildea, J. A. K. Howard and H. Puschmann, *J. Appl. Crystallogr.*, 2009, **42**, 339–341.
23 G. M. Sheldrick, *Acta Crystallogr., Sect. A:Found. Adv.*, 2015, **71**, 3–8.
24 Inc Wavefunction, *Spartan'14*, Inc Wavefunction, Irvine, CA, USA, 2013.
25 M. J. Frisch, G. W. Trucks, H. B. Schlegel, G. E. Scuseria, M. A. Robb, J. R. Cheeseman, G. Scalmani, V. Barone, B. Mennucci and G. A. Petersson, *Gaussian 09*, Revision A.1, Gaussian Inc, Wallingford, CT, USA, 2009.
26 T. Bruhn, A. Schaumlöffel, Y. Hemberger and G. Bringmann, *SpecDis*, version 1.53, University of Würzburg, Würzburg, Germany, 2012.
27 L. Zhou, X. Chen, C. Sun, Y. Chang, X. Huang, T. Zhu, G. Zhang, Q. Che and D. Li, *Mar. Drugs*, 2021, **19**, 575.
28 Z. Y. Zhou, R. Liu, M. Y. Jiang, L. Zhang, Y. Niu, Y. C. Zhu, Z. J. Dong and J. K. Liu, *Chem. Pharm. Bull.*, 2009, **57**, 975–978.
29 R. Li, S. Chen, S. Niu, L. Guo, J. Yin and Y. Che, *Fitoterapia*, 2014, **96**, 88–94.
30 A. O. Noor, D. M. Almasri, A. A. Bagalagel, H. M. Abdallah, S. G. A. Mohamed, G. A. Mohamed and S. R. M. Ibrahim, *Molecules*, 2020, **25**, 395.
31 C. Wang, H. Xu, J. Wang, C. Wei, S. Zheng, R. Xu, S. Wang, Z. Li, P. Li and F. Kong, *J. Nat. Prod.*, 2025, **88**, 757–767.
32 P. Wang, H. Wang, J. Yang, L. Yang, C. Cai, J. Yuan, F. Wu, C. Gai, W. Mei and H. Dai, *Mar. Drugs*, 2023, **21**, 150.
33 G. Shabir, A. Saeed and H. R. El-Seedi, *Phytochemistry*, 2021, **181**, 112568.
34 CCDC 2443606: Experimental Crystal Structure Determination, 2026, DOI: 10.5517/ccdc.csd.cc2n0s0h.